BIOENGINEERING

Wearable/disposable sweat-based glucose monitoring device with multistage transdermal drug delivery module

Hyunjae Lee,[1,2]* Changyeong Song,[1,2]* Yong Seok Hong,[1,2] Min Sung Kim,[1,2] Hye Rim Cho,[1,3] Taegyu Kang,[1,2] Kwangsoo Shin,[1,2] Seung Hong Choi,[1,3] Taeghwan Hyeon,[1,2†] Dae-Hyeong Kim[1,2†]

Electrochemical analysis of sweat using soft bioelectronics on human skin provides a new route for noninvasive glucose monitoring without painful blood collection. However, sweat-based glucose sensing still faces many challenges, such as difficulty in sweat collection, activity variation of glucose oxidase due to lactic acid secretion and ambient temperature changes, and delamination of the enzyme when exposed to mechanical friction and skin deformation. Precise point-of-care therapy in response to the measured glucose levels is still very challenging. We present a wearable/disposable sweat-based glucose monitoring device integrated with a feedback transdermal drug delivery module. Careful multilayer patch design and miniaturization of sensors increase the efficiency of the sweat collection and sensing process. Multimodal glucose sensing, as well as its real-time correction based on pH, temperature, and humidity measurements, maximizes the accuracy of the sensing. The minimal layout design of the same sensors also enables a strip-type disposable device. Drugs for the feedback transdermal therapy are loaded on two different temperature-responsive phase change nanoparticles. These nanoparticles are embedded in hyaluronic acid hydrogel microneedles, which are additionally coated with phase change materials. This enables multistage, spatially patterned, and precisely controlled drug release in response to the patient's glucose level. The system provides a novel closed-loop solution for the noninvasive sweat-based management of diabetes mellitus.

INTRODUCTION

Diabetes is one of the most prevalent chronic diseases, causing uncontrollable blood glucose levels (*1*). Patients with diabetes are advised to check their blood glucose level daily and to take periodic insulin shots for continuous management of their blood glucose level (*2*). However, patients often do not follow this recommendation because of the pain and accompanying intense stress of repetitive blood collection and insulin shots. This often leads to various severe diabetic complications, such as cardiovascular and kidney diseases, stroke, blindness, and nerve degeneration. In addition, insulin overtreatment causes an abrupt drop in the blood glucose concentration, which may cause seizures, unconsciousness, and even death. Therefore, a novel method for painless and stress-free glucose monitoring (*3*–*5*) and precise maintenance of homeostasis through controlled drug delivery (*6*, *7*) is highly desirable.

Extensive efforts have been made to develop noninvasive sweat-based biomarker monitoring methods. Wearable biosensors enable continuous monitoring of metabolites [including glucose (*3*–*5*), lactate (*8*), and alcohol (*9*)] and electrolytes [including potassium (*3*), calcium (*10*), and heavy metal ions (*11*)] in sweat. The estimation of the blood glucose concentration based on the sweat-based glucose measurement is a potential solution (*12*, *13*). However, many challenges still exist for the accurate sweat-based glucose measurement (*14*, *15*). For example, the sweat collection procedure is tedious, and the sweat collection times vary depending on environmental conditions. In addition to the difficulty of measuring glucose levels in sweat because of its much smaller concentration than that in blood, lactic acid in sweat, ambient temperature changes, and various medications can induce errors in enzyme-based glucose sensing. Mechanical friction and deformation of devices on soft human skin can delaminate the enzyme from the glucose sensor and cause mechanical fractures in devices. A closed-loop system with the feedback delivery of a precisely controlled amount of drugs in response to the glucose monitoring result is another important unaccomplished goal for maintaining homeostasis (*6*, *7*).

Various kinds of flexible and stretchable devices based on an ultrathin (*16*–*18*) and stretchable design (*19*, *20*) have been developed for monitoring individual health status and delivering the corresponding feedback therapy (*21*, *22*). Here, we develop a patch-based wearable/strip-type disposable system for noninvasive sweat glucose monitoring and microneedle-based point-of-care therapy (*23*). Key novel advantages of this system include (i) mass production–compatible porous metal-based electrodes and fabrication processes, (ii) miniaturized sensor design that allows for reliable sweat analysis even with an infinitesimal amount of sweat, (iii) patch- and disposable-type design for enhancing practical applicability, (iv) multiple sweat control and uptake layers for efficient sweat collection, (v) a porous gold nanostructure for maximizing the electrochemically active surface area for detection of a small amount of glucose in sweat with high sensitivity, (vi) multiple glucose sensing devices for enhanced accuracy, and (vii) multistage and precisely controlled transdermal drug [metformin or chlorpropamide (type 2 diabetes drugs)] delivery through biocompatible hyaluronic acid hydrogel microneedles containing drug-loaded phase change nanoparticles (PCNs). Metformin is one of the first-line drugs for treating type 2 diabetes (*24*). Because drug delivery through the skin can bypass the digestive system, transdermal delivery of metformin requires a lower dosage of drugs than oral delivery and prevents

[1]Center for Nanoparticle Research, Institute for Basic Science, Seoul 08826, Republic of Korea. [2]School of Chemical and Biological Engineering, Institute of Chemical Processes, Seoul National University, Seoul 08826, Republic of Korea. [3]Department of Radiology, Seoul National University College of Medicine, Seoul 03080, Republic of Korea.
*These authors contributed equally to this work.
†Corresponding author. Email: dkim98@snu.ac.kr (D.-H.K.); thyeon@snu.ac.kr (T.H.)

gastrointestinal side effects (*23*). This novel system for high-fidelity sweat glucose measurement and feedback-controlled drug delivery enables efficient management of blood glucose concentration without pain and stress.

RESULTS

System design of the wearable diabetes patch and disposable strip

The patch-based wearable devices in Fig. 1A have an ultrathin and stretchable design (fig. S1A), which enables conformal contact with the skin for efficient sweat collection and high performance under physical deformation. The same sensors can be further miniaturized and fabricated as a disposable strip (Fig. 1B). Depending on the sweat glucose concentration, an appropriate amount of metformin (or chlorpropamide) is transdermally delivered through microneedles. The drug delivery can be thermally controlled in a multistage manner. The microneedles assembled on the multichannel thermal actuator can be periodically replaced with new ones (Fig. 1C and fig. S1, B and C). These patch-type devices are fabricated on a handle substrate and then transfer-printed onto a thin silicone patch (fig. S2). The strip-type sensor is fabricated on a thin polyimide (PI) substrate. Patterned electrochemical functionalization completes the fabrication.

The system operation sequence is schematically described in fig. S3. After wearing the patch, sweat accumulates in the porous sweat-uptake layer. A waterproof band behind the silicone patch aids in sweat collection and prevents delamination of the patch from the skin. A porous and negatively charged Nafion layer between the sensors and the

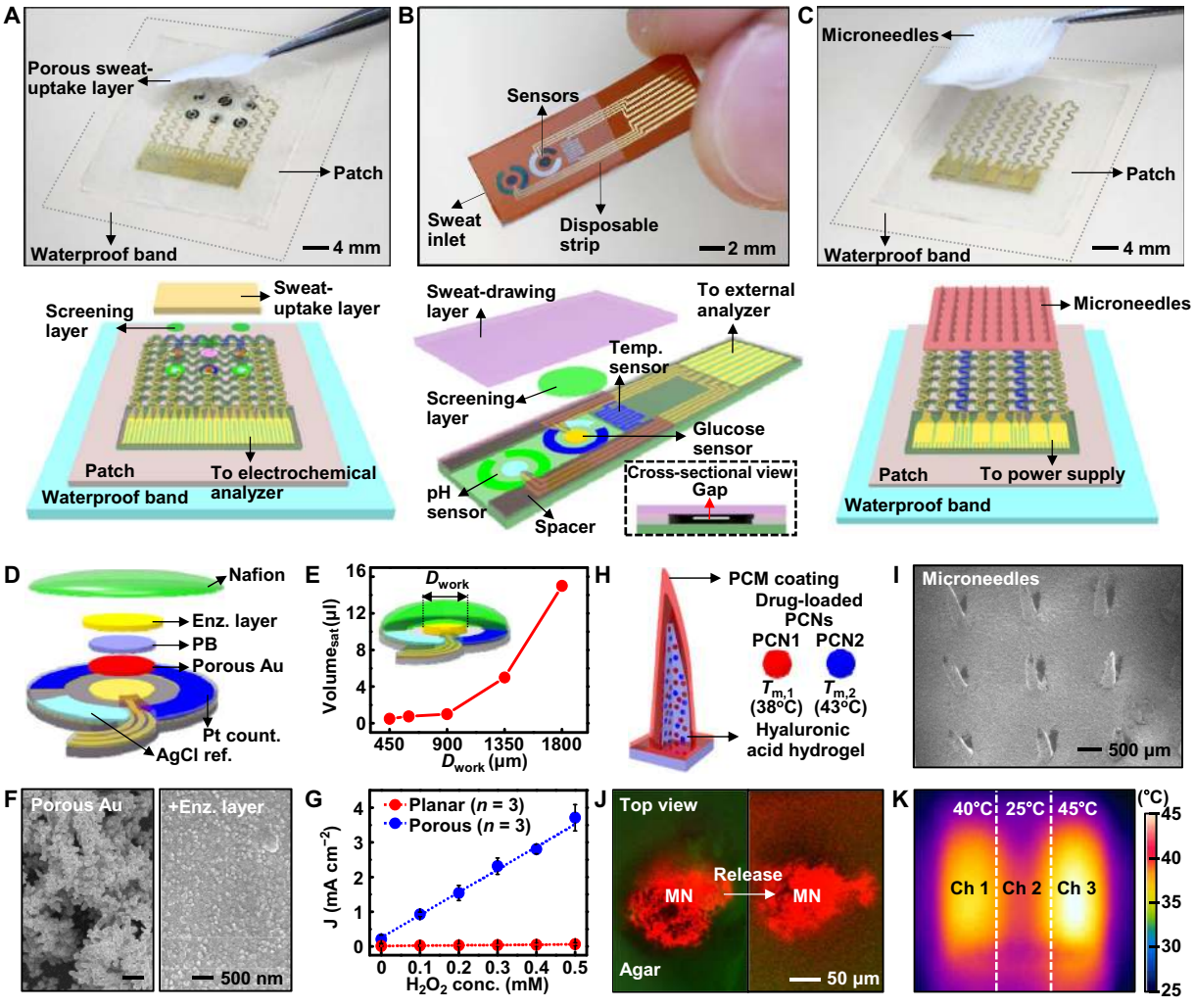

Fig. 1. Wearable/disposable sweat monitoring device and microneedle-based transdermal drug delivery module. (**A**) Optical camera image (top; dotted line, edges of the patch) and schematic (bottom) of the wearable sweat monitoring patch. A porous sweat-uptake layer is placed on a Nafion layer and sensors. (**B**) Optical camera image (top) and schematic (bottom) of the disposable sweat monitoring strip. (**C**) Optical camera image (top; dotted line, edges of the patch) and schematic (bottom) of the transdermal drug delivery device. Replacement-type microneedles are assembled on a three-channel thermal actuator. (**D**) Schematic drawing of the glucose sensor in an exploded view. PB, prussian blue. (**E**) Minimum volume of the artificial sweat required for sensing with different sizes of the glucose sensor. (**F**) Scanning electron microscope (SEM) images before (left) and after (right) immobilization of the enzyme (enz.) on the porous gold electrode. (**G**) Comparison of the H_2O_2 sensitivity in the planar and porous gold electrode deposited with Prussian blue at different H_2O_2 concentrations. (**H**) Schematic of the drug-loaded microneedles. The right inset describes details of different PCNs. (**I**) SEM image of the microneedles. (**J**) Confocal microscope images of the released dye from microneedles (MN) (top view) into the 4% agarose gel (green, agar; red, dye). (**K**) Infrared (IR) camera image of the three-channel (ch) thermal actuator.

sweat-uptake layer helps in the immobilization of the enzyme (*25*) and screens out negatively charged molecules that may affect the glucose sensing (for example, drug molecules contained in sweat, such as acetaminophen or acetylsalicylic acid) (*25*, *26*). A humidity sensor monitors the critical amount of sweat for reliable glucose sensing by measuring impedance change by sweat generation. Above the critical humidity, the glucose, pH, and temperature sensors begin taking measurements to determine correlated blood glucose level. The pH and temperature sensors correct potential errors of the enzyme-based glucose level measurement in real time. Upon hyperglycemia, thermal actuation controls the feedback transdermal delivery of metformin loaded in PCNs.

Materials and key device design

A series of stretchable sensors (humidity, glucose, pH, and temperature) are monolithically integrated (Fig. 1A) for efficient sweat-based glucose sensing. Multipoint sensing for glucose (triple) and pH (quadruple) improves the detection accuracy (fig. S1A). In the glucose and pH sensors, the reference and counter electrodes are designed to be packed as closely as possible to minimize the required amount of sweat (Fig. 1D). As the working electrode diameter (D_{work}) decreases, the required sweat amount can be reduced to as small as 1 μl (Fig. 1E), which is a 20-fold decrease from that previously reported by Lee *et al.* (*5*). The working electrode consists of porous gold formed by electrodeposition and enzymes [glucose oxidase (GOx)] drop-casted on it and then covered by Nafion and sequentially cross-linked by glutaraldehyde (Fig. 1F). The porous structure allows for a larger electrochemically active surface area (*27*, *28*) and stronger enzyme immobilization (*29*, *30*). Cyclic voltammograms (fig. S4A) and ac impedance measurements (fig. S4, B and C) using the $Fe(CN)_6^{3-/4-}$ redox couple show a high charge storage capacity and low interfacial impedance in the porous structure. The high H_2O_2 reducing catalytic activity of the porous structure (Fig. 1G and fig. S4D) confirms the enhanced sensitivity. Robustly cross-linked enzymes on the porous metal structure also enhance the reliability of the sensor under mechanical friction and deformation.

Film-type microneedles (fig. S1B) are integrated on top of the stretchable heater (fig. S1C), and these needles can be periodically replaced (Fig. 1C). For the multistep and precisely controlled drug delivery, two types of metformin-loaded PCNs [PCN1, melting transition temperature ($T_{m,1}$) = 38°C; PCN2, $T_{m,2}$ = 43°C] are embedded in the hyaluronic acid hydrogel microneedles (Fig. 1H). The hyaluronic acid hydrogel is a widely used biocompatible material (*31*). An additional coating with phase change materials (PCMs) prevents unwanted dissolution of the hyaluronic acid matrix in contact with interstitial fluids (Fig. 1H). Controlled thermal actuation by the integrated heater activates either PCN1 alone or both PCNs (fig. S5). An SEM image of the fabricated microneedles is shown in Fig. 1I. Confocal microscope images show the dye release from microneedles into 4% agarose gel (tissue-like gel) (Fig. 1J) (*32*). The heater is designed with three channels (Fig. 1K) and triggers the multistage drug delivery that can be tuned with thermal patterns.

Sweat control optimization

Efficient use of the generated sweat is an important issue in the sweat-based monitoring system, which is enabled by the sweat-uptake and waterproof layers. A porous and hydrophilic sweat-uptake layer (Fig. 2A, inset) (*33*, *34*), which is placed on the Nafion layer and sensors, absorbs sweat and delivers it to the sensors through the Nafion layer (fig. S6A). The waterproof band added on the elastomeric silicone patch covers the outside to separate the sweat from external humidity (Fig. 2A), suppresses sweat evaporation (fig. S6B), and prevents delamination of the patch during skin deformation (Fig. 2B). The strip-type sensor absorbs sweat by the capillary force formed by the gap (fluidic channel) between the sweat-drawing layer and substrate (Figs. 1B, bottom inset, and 2C). The miniaturized sensor design (Fig. 1, D and E) and the fast collection of sweat enable rapid sensing. The miniaturized glucose sensor can be stably operated with only 1 μl of sweat (Fig. 2D and fig. S6, C and D).

Electrochemical and electrical characterization of individual sensors

The humidity sensor monitors the sweat collection procedure through impedance changes of poly(3,4-ethylenedioxythiophene) (PEDOT) interdigitated electrodes to estimate an appropriate starting point of sweat analysis (Fig. 2E). The glucose sensor based on a Prussian blue–deposited porous gold electrode is calibrated to the glucose concentration range between 10 μM and 1 mM (typical glucose concentrations in human sweat) by the galvanostatic method (Fig. 2F and fig. S7, A and B). These glucose concentrations correspond to typical sweat glucose concentrations of both hypoglycemic and hyperglycemic patients as well as healthy people (*12*, *13*). The glucose sensor is stable under mechanical deformation (fig. S7C) and selectively detects glucose in the presence of other biomolecules [including ascorbic acid, uric acid, and lactic acid (*3*, *35*)] and drugs [including acetaminophen, acetylsalicylic acid, and metformin (fig. S7D) (*36*–*38*)], whose concentrations are in values commonly found in the human sweat. The glucose sensor works for one full day without additional calibration under ambient conditions and for several days depending on storage conditions (fig. S7E).

The enzyme-based glucose sensor shows deviations at different pH levels (fig. S7F), and thus simultaneous monitoring of pH levels is important. The pH sensor measures changes in the open circuit potential (OCP) between a polyaniline (PANi)–deposited working electrode and an Ag/AgCl electrode. The pH sensor is calibrated using standard pH buffer solutions (Fig. 2G and fig. S8A) and maintains stable operation under deformation (fig. S8B). Because the dependence of measured OCP and the pH was not linear, the calibration curves were obtained for every pH difference of 0.5. The pH sensor is reliable over repeated use at different pH levels (fig. S8C) and different temperatures (fig. S8D). The resistor-based temperature sensor is also calibrated for skin temperature monitoring (Fig. 2H). The simultaneous use of these co-integrated sensors can enhance the accuracy of glucose sensing. For example, metabolic secretion of lactic acid in sweat lowers the pH level to 4 to 5. The simultaneous pH sensing can correct this pH-dependent deviation (Fig. 2I and fig. S7F) of the enzyme-based glucose sensor. Simulated hyperglycemia—0.3 mM sweat glucose—is monitored in vitro under two different pH variation settings (5→4→5 and 5→6→5; Fig. 2J, left and right). In both cases, real-time correction increases glucose measurement accuracy. The glucose sensor with the current device setting does not show significant deviations at different temperatures (Fig. 2K).

Thermoresponsive PCNs

PCMs have melting temperatures that are low but above human body temperature, and thus they are widely used in the thermoresponsive drug delivery (*39*). PCNs are made of PCMs, drugs, and biocompatible ligands (Fig. 3A). Different PCNs enable temperature-dependent stepwise drug delivery. We use palm oil (PCN1, T_m = 38°C) and tridecanoic acid (PCN2, T_m = 43°C), which melt above the skin temperature

(30°C; fig. S9A). The drugs (metformin or chlorpropamide) are embedded in the PCM matrix (Fig. 3A and fig. S9, B to D). Pluronic F-127 and 3,4-dihydroxyl-L-phenylalanine (DOPA)–conjugated hyaluronic acid (fig. S10, A and B) are used as ligands, which make an oil-in-water emulsion (fig. S11A). Cryogenic transmission electron microscopy (cryo-TEM) images show that PCNs below the melting temperature are solid (Fig. 3, B and C, left). Above the melting temperature, PCNs change to liquid and aggregate (Fig. 3, B and C, right). Cytotoxicity tests show that both PCNs are nontoxic and suitable for biomedical applications (fig. S11B). The hydrodynamic diameters and negative zeta potentials of the PCNs slightly increase and decrease, respectively, as the temperature increases from the skin temperature (30°C; fig. S9A) to above melting temperatures (40° and 45°C; Fig. 3D and fig. S11C). The PCM matrices can block the drug release before thermal actuation. Their stepwise temperature-dependent melting controls the amount of the drug release. When the temperature reaches 40°C, only the drugs contained in PCN1 are released, whereas at 45°C, the drugs in both PCN1 and PCN2 are released (fig. S11D).

Microneedle fabrication and multistage drug delivery

The microneedles are fabricated by molding the hyaluronic acid hydrogel matrix containing drug-loaded PCNs, followed by an additional PCM spray coating (Fig. 3E, left, and fig. S12). A confocal laser fluorescence microscope image shows that the dye-loaded PCNs are well embedded in the microneedles (Fig. 3E, right). Hydrogel-based microneedles dissolve when they come in contact with body fluids (Fig. 3F, left), whereas the PCM coating prevents the dissolution before the controlled melting of the PCM (Fig. 3F, right). The microneedles should be stiff enough to penetrate into the skin (*40*); compression tests confirm their mechanical strength (Fig. 3G). The microneedles successfully penetrate into 4% agarose gel (tissue-like gel) and generate pores (Fig. 3H, left). After poration by microneedles, vertical heat transfer dissolves the outside PCM coating and embedded PCNs. Although accidental peel-offs create small defects in the PCM coating, the drug contained in the PCNs is not released. The vertical temperature distribution of the agarose gel imaged by an IR camera confirms the successful heat transfer (Fig. 3H, right). To investigate the stepwise

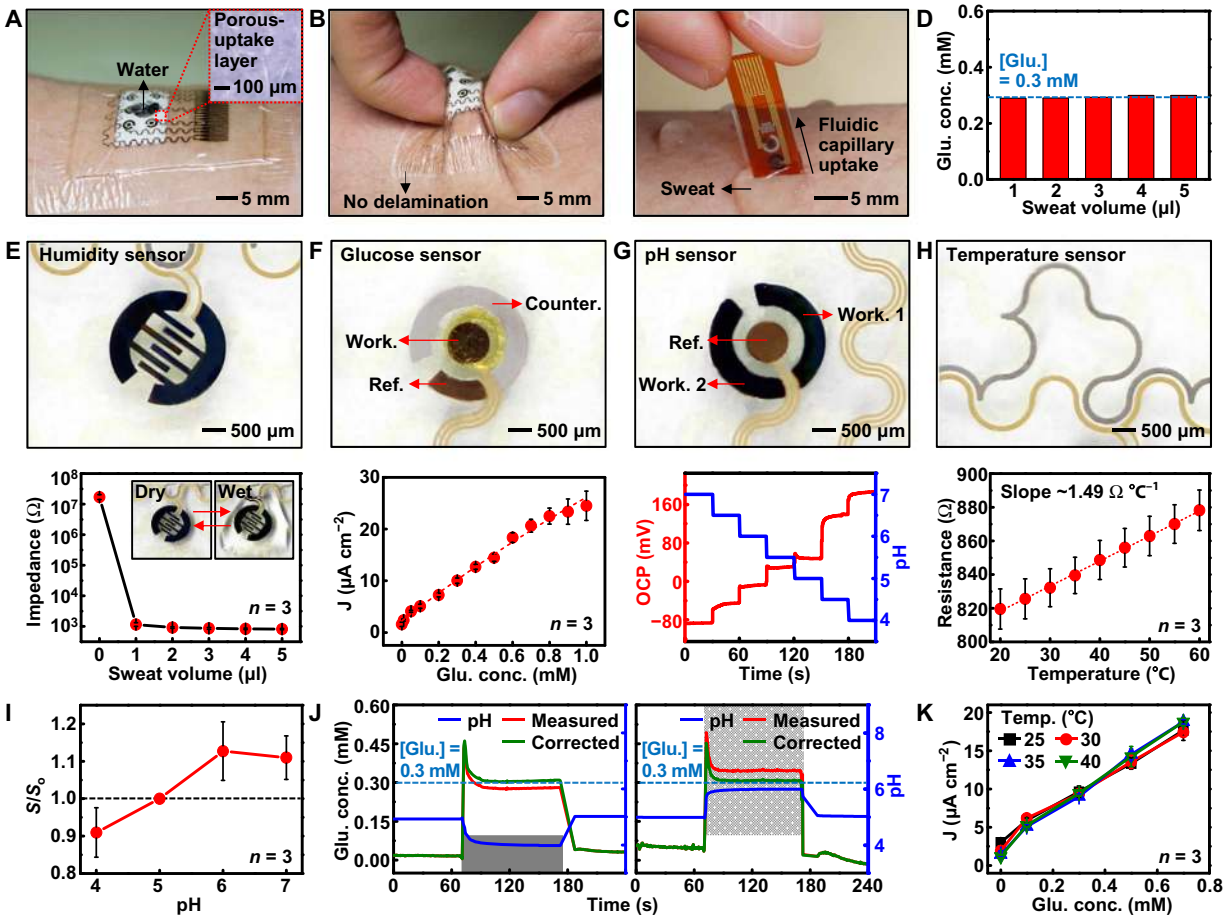

Fig. 2. Optimization of the sweat control and characterization of individual sensors. (**A**) Optical image of the wearable sweat analysis patch with a sweat-uptake layer and a waterproof band. The inset shows the magnified view of the porous sweat-uptake layer. (**B**) Optical image of the sweat analysis patch under deformation. (**C**) Optical image of the disposable sweat analysis strip on human skin with perspiration. (**D**) Glucose (glu.) concentration measurement at different sweat volumes (0.3 mM glucose in artificial sweat). (**E**) Optical image (top) and calibration curve (bottom) of the humidity sensor. Inset shows the image before and after wetting of the sensor. (**F**) Optical image (top) and calibration curve (bottom) of the glucose sensor. (**G**) Optical image (top) and calibration curve (bottom) of the pH sensor. (**H**) Optical image (top) and calibration curve (bottom) of the temperature sensor. (**I**) Changes of the relative sensitivity of the uncorrected glucose sensor at different pH levels. The relative sensitivity (S/S_o) is defined as measured sensitivity divided by sensitivity at pH 5. (**J**) In vitro monitoring of glucose changes with (green) and without (red) correction using simultaneous pH measurements (blue). (**K**) Calibration curves of the glucose sensor at different temperatures.

drug release, we heated the microneedles containing dyes from 25° to 45°C (Fig. 3I). There is a negligible release under and around the skin temperature (30°C) due to the PCM coating and PCNs. At the elevated temperature (40°C), the PCM coating on microneedles and PCN1 are dissolved, and metformin in PCN1 is released. At the higher temperature (45°C), metformin in both PCN1 and PCN2 is released. Spatial patterning of the embedded heater subdivides the release steps further, which is precisely controlled (fig. S13A) by co-integrated temperature sensors (fig. S13, B and C). Heaters consisting of the three channels together with the two types of PCNs result in eight different spatiothermal patterns (Fig. 3J) and six-stage programmed dye-release profiles (Fig. 3K).

Sweat-based glucose monitoring on human subjects

Wearable/disposable sweat-based glucose sensors are used for human sweat analysis. The wearable patch is connected to a portable electrochemical analyzer (Fig. 4A and fig. S14). The monitoring starts with humidity sensing to determine the optimum point to start sweat analysis (Fig. 4B). When the sweat-uptake layer absorbs a sufficient amount of sweat, the glucose and pH sensors detect the sweat glucose and pH levels, respectively. The triple glucose and quadruple pH sensing (fig. S1A) improve the detection accuracy (Fig. 4C). The correction using the measured pH enables more accurate glucose sensing (Fig. 4D). The patch works reliably under different skin temperatures (temperature range, 30° to 37°C) before, during, and after physical movements (fig. S15, A and B). The changes of skin temperature with the current experimental setting are small because of homeostatic functions of the nervous system (*41*). The patch is reusable and/or reattachable multiple times (fig. S15, C and D).

The disposable strip-type sensor is more convenient for the sweat analysis. The strip-type sensor first absorbs sweat (Fig. 2C) because of the capillary effect, and it is then connected to the hardware for sweat analysis through a ZIF connector (Fig. 4E). The absorbed sweat should cover the surface of both pH and glucose sensors (Fig. 4F). The amount of absorbed sweat can be monitored by measuring the impedance between the electrodes of the glucose sensor (Pt counter electrode and Ag/AgCl reference electrode) and those of the pH sensor (two PANi-deposited working electrodes) (Fig. 4G). The strip-type sensor can be stably operated with 4 μl of sweat (fig. S16A). When the sweat covers both glucose and pH sensors, the measurements begin (Fig. 4H). The calibration curves for a strip-type device are shown in fig. S16 (B and C).

The sweat pH levels vary among subjects and depending on the physiological conditions of each subject (fig. S17A). The sweat glucose levels corrected by pH measurements before and after a meal agree well with the sweat glucose levels measured among subjects using a commercial glucose assay kit (Fig. 4I). Statistical analysis confirms the reliable correlation of sweat glucose levels measured by the wearable and disposable sweat glucose sensors with the blood glucose levels measured by a commercial glucose meter (fig. S17B). For the accurate estimation of the blood glucose level based on the sweat glucose level, the correlation factor between the glucose concentration of blood and sweat should be found for each individual subject with enough data (fig. S17C). With this data, it is clear that blood glucose concentration tends to vary before and after a meal, similarly to the measured sweat glucose concentration (Fig. 4J).

Controlled transdermal drug delivery using microneedles

Transdermal drug delivery experiments based on the fabricated microneedles and integrated heaters in vivo are conducted on 8-to-12-week-old

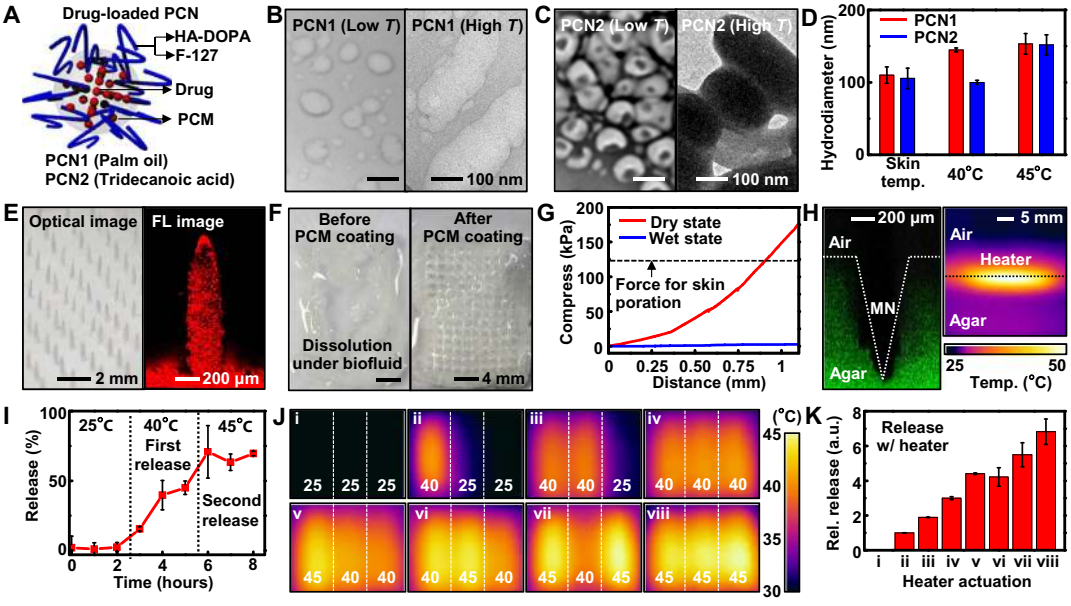

Fig. 3. Characterization of PCNs and PCN-loaded microneedles. (**A**) Schematic illustration of the PCN. HA, hyaluronic acid. (**B**) Cryo-TEM image of PCN1 (palm oil) below the melting temperature (left) and TEM image of PCN1 above the melting temperature (right). (**C**) Cryo-TEM image of PCN2 (tridecanoic acid) below the melting temperature (left) and TEM image of PCN2 above the melting temperature (right). (**D**) Dynamic light scattering size measurement of PCNs at 30° (skin temperature), 40°, and 45°C. (**E**) Optical image (left) and confocal fluorescence (FL) microscope image (right) of PCM-coated microneedles. Microneedles contain dye-loaded PCNs for imaging. (**F**) Microneedle dissolution test in PBS before (left) and after (right) the PCM coating. (**G**) Mechanical strength test of microneedles in their dry and wet states. (**H**) Confocal microscope image of microneedles penetrating into 4% agarose gel (left) and IR camera image of the thermal actuation on the gel (right). (**I**) Drug-release profile from microneedles. (**J**) IR camera images of eight different spatiothermal profiles using the three-channel thermal actuator for multistage drug delivery. (**K**) Multistage drug-release profile. a.u., arbitrary units.

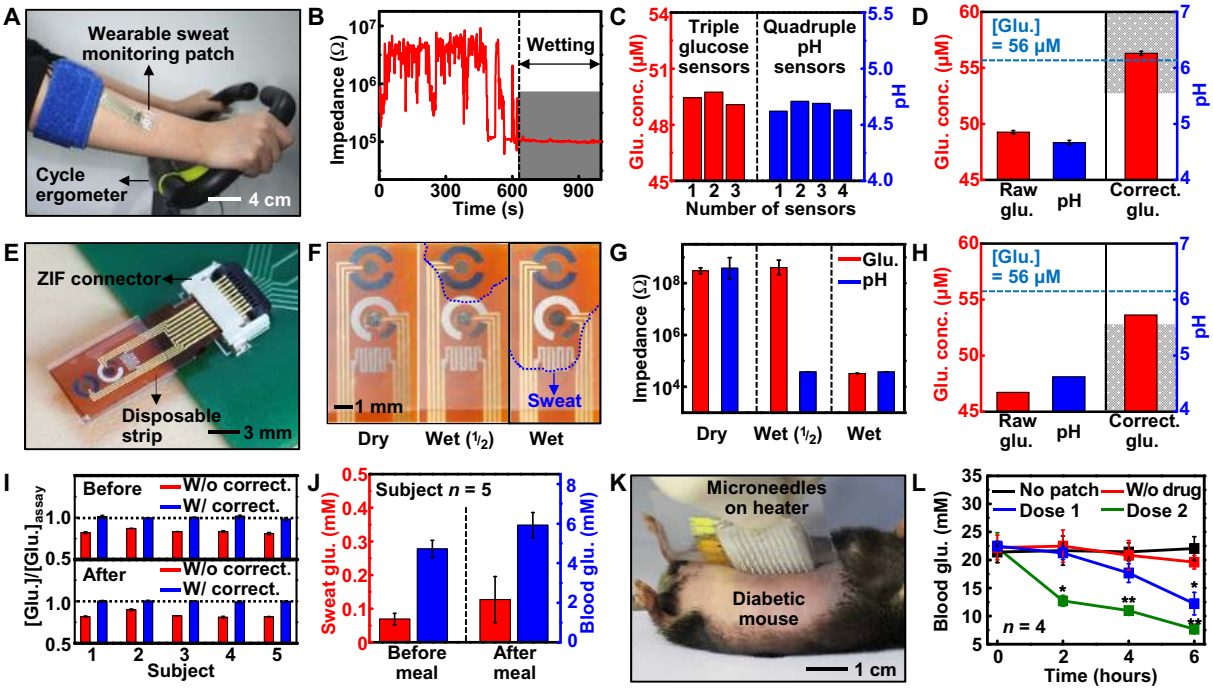

Fig. 4. Sweat-based glucose monitoring and feedback therapy in vivo. (**A**) Optical camera image of the subject using a cycle ergometer for sweat generation with the wearable patch on the subject's arm. (**B**) Real-time humidity monitoring to check the accumulation of sweat. (**C**) Multimodal glucose and pH sensing to improve detection accuracy. (**D**) Measured sweat glucose concentrations (n = 3), pH levels (n = 4), and corrected sweat glucose level (n = 3) based on the averaged pH (dotted line, glucose concentration measured by a commercial glucose assay). (**E**) Optical camera image of the disposable strip-type sensors connected to a zero insertion force (ZIF) connector. (**F**) Optical camera images of the sweat uptake via the fluidic channel of the strip. (**G**) Humidity monitoring of the disposable strip using impedance measurements. (**H**) Sweat glucose and pH monitoring using the disposable strip. (**I**) Ratio of sweat glucose concentrations (n = 3) measured by the patch and a commercial glucose assay with and without the pH-based correction before and after a meal. (**J**) Comparison of the sweat and blood glucose concentrations before and after a meal. (**K**) Optical camera image of the transdermal drug delivery device on the db/db mouse. (**L**) Blood glucose levels of the db/db mice for the treated groups (microneedles with the drugs) and control groups (without the patch, microneedle without the drugs) (*P < 0.05, **P < 0.01 versus control, Student's t test).

diabetic (db/db) mice (type 2 diabetes mellitus model). The in vivo treatment starts with lamination of a therapeutic patch on the shaved abdomen of the db/db mouse (Fig. 4K). Trypan blue staining on the mouse skin confirms that the microneedles can successfully penetrate the skin for the drug (metformin) delivery (fig. S18A). The integrated heaters modulate the amount of the drug delivery by the controlled thermal actuation (fig. S18B). Control groups that have no patch (black), microneedles without diabetes drugs (red), and microneedles with diabetes drugs (blue, dose 1; green, dose 2) are used (Fig. 4L). The experimental groups (blue and green) show significant decrease in blood glucose level compared to the control groups (black and red). As more metformin is delivered to the db/db mice, the blood glucose level is suppressed more. The blood glucose concentration of the measurement group (dose 2, green) decreased to 7.6 mM, which is a normoglycemic state (<11 mM).

DISCUSSION

We report a novel material structure, device design, and system integration strategy for a sweat glucose monitoring device integrated with feedback transdermal drug delivery microneedles. Depending on the design, the device can be either wearable-patch type or disposable-strip type. For efficient sweat control and sensing, the sweat monitoring patch is assembled with multiple sweat-uptake and waterproof layers, and sensor sizes are miniaturized to the point that ~1 μl of sweat is sufficient for reliable measurement. The measurements of sweat glucose levels with real-time correction based on pH, temperature, and humidity sensing are accurate under various environment changes. The sweat glucose data are well correlated with the blood glucose levels. For precise and timely drug delivery, two types of metformin-loaded PCNs are embedded in the PCM-coated microneedles. The thermoresponsive microneedles controlled by multichannel heaters enable the multistage and spatially patterned transdermal drug release in response to the measured sweat glucose level.

For practical application of the current system, there are several things to improve. The long-term stability and uniformity of sensors are particularly important to make the system practically applicable to human subjects with minimum recalibrations. Further studies about the correlation between glucose levels of blood and sweat are needed before application to diabetic patients. Although metformin used in the system shows slow suppression of the blood glucose levels due to its working mechanism (*42*), another kind of drug (for example, chlorpropamide) can be loaded for synergistic treatment or fast regulation of blood glucose level. With further improvements in these points, clinical translation can be pursued for sweat-based sensing and feedback therapy. The current system provides important new advances toward the painless and stress-free point-of-care treatment of diabetes mellitus.

MATERIALS AND METHODS

Fabrication process of the device array

The wearable device fabrication began with spin-coating of the PI precursor (~1.5 μm; product #575798, Sigma-Aldrich) on a SiO_2 wafer,

followed by thermal curing of the PI. A Cr/Au thin film (~30 nm/~70 nm) was deposited on electrodes by thermal evaporation. The Cr/Au thin film was patterned by photolithography and wet etching. A Cr/Pt thin film (~10 nm/~100 nm) was deposited by sputtering and patterned by photolithography for the temperature sensor and the counter electrode of the glucose sensor. The top epoxy layer (~1.5 μm; SU8-2, MicroChem) was coated and patterned by photolithography. The bottom PI layer was selectively isolated by photolithography and reactive-ion etching. The device was transfer-printed onto a polydimethylsiloxane (PDMS) substrate (Sylgard 184, Dow Chemical) using a water-soluble tape (product #5414, 3M). The strip-type device was fabricated on the PI film (125 μm; Isoflex) using the same procedures.

Functionalization of sensors and electrodes with electrochemically active materials

(i) PEDOT electrodeposition. A solution of 0.01 M 3,4-ethylenedioxythiophene (product #483028, Sigma-Aldrich) and 0.1 M $LiClO_4$ (product #271004, Sigma-Aldrich) in acetonitrile (product #271004, Sigma-Aldrich) was prepared. The gold electrode was dipped in the solution, and galvanostatic electrodeposition was performed for 40 s at 1.2 V (potential versus commercial Ag/AgCl electrode).

(ii) Ag/AgCl electrodeposition. An aqueous solution of 5 mM $AgNO_3$ (product #209139, Sigma-Aldrich) and 1 M KNO_3 (product #P8394, Sigma-Aldrich) was prepared. The gold electrode was dipped in the prepared solution. The potential was swept from −0.9 to 0.9 V versus a Ag electrode for 14 segments at a scan rate of 0.1 V s^{-1}. For chlorination, the electrode was dipped in an aqueous solution of 0.1 M KCl (product #P5405, Sigma-Aldrich) and 0.01 M HCl (product #H1758, Sigma-Aldrich). The potential was swept from −0.15 to 1.05 V versus a commercial Ag/AgCl electrode for four segments at a scan rate of 0.05 V s^{-1}.

(iii) Porous gold electrodeposition. An aqueous solution of 2 mM $HAuCl_4$ (product #70-0500, Strem Chemicals) in 2 M H_2SO_4 (product #320501, Sigma-Aldrich) was prepared. The gold electrode was dipped in the prepared solution. The porous gold was electrodeposited by the galvanostatic method for 5 min at −1 V with a Pt counter electrode and a commercial Ag/AgCl electrode (total charge, ~0.5 C).

(iv) Prussian blue electrodeposition. An aqueous solution of 10 mM KCl, 2.5 mM $K_3[Fe(CN)_6]$ (product #P702587, Sigma-Aldrich), and 2.5 mM $FeCl_3{\cdot}6H_2O$ (product #236489, Sigma-Aldrich) in 0.1 M HCl was prepared. The gold electrode was dipped in the solution, and the potential was swept from 0 to 0.5 V versus a commercial Ag/AgCl for two segments at a scan rate of 0.02 V s^{-1}.

(v) GOx immobilization. 1 weight % (wt %) chitosan (product #C3646, Sigma-Aldrich) solution was prepared by dissolving the chitosan in 2 wt % acetic acid (product #695092, Sigma-Aldrich). The chitosan solution was mixed with an exfoliated graphite (product #282863, Sigma-Aldrich) solution (2 mg ml^{-1}) in 1× phosphate-buffered saline (Dulbecco's PBS, WELGENE Inc.). The exfoliation process was conducted using an ultrasonic machine (Sonics VCX-750, Vibra-Cell) for 30 min. The chitosan/graphene solution was mixed with GOx (0.05 g ml^{-1}; product #G7141, Sigma-Aldrich) and bovine serum albumin (BSA) (0.01 g ml^{-1}; product #A2153, Sigma-Aldrich). A solution of GOx (0.05 g ml^{-1}) and BSA (0.01 g ml^{-1}) was also prepared in 1× PBS. GOx and BSA (0.8 μl) in a PBS solution was drop-casted on the porous gold–deposited electrode. After drying the electrodes under ambient conditions, 0.8 μl of GOx in the chitosan/graphene solution was drop-casted on the electrode. After drying the electrodes under ambient conditions, 2 μl of 0.5 wt % Nafion (product #309389, Sigma-Aldrich) was drop-casted on the glucose sensor. After drying of Nafion under ambient conditions, 0.8 μl of 2 wt % glutaraldehyde (product #G5882, Sigma-Aldrich) was drop-casted on the glucose sensor for robust cross-linking of the enzyme layer.

(vi) PANi electrodeposition. An aqueous solution of 0.1 M aniline (product #242284, Sigma-Aldrich) in 1 M HCl was prepared. The gold electrode was dipped into the solution, and the potential was swept from −0.2 to 1 V versus a commercial Ag/AgCl electrode for 60 segments at a scan rate of 0.1 V s^{-1}.

Fabrication of microneedles

A female PDMS (Sylgard 184, Dow Chemical) mold was prepared on the basis of commercial microneedles (PAMAS, Prestige). The microneedles have a height of 1 mm and a round base diameter of 250 μm. The drug-loaded PCNs [metformin (product #D150959, Sigma-Aldrich) or chlorpropamide (product #C129531, Aladdin)] and a 2% hyaluronic acid solution were drop-casted on the PDMS mold. The sample was placed under vacuum until no bubble was generated. After degassing, the sample was dried at room temperature. The microneedles were carefully peeled from the mold. The PCM (tetradecanol; product #185388, Sigma-Aldrich) was sprayed on the microneedles. The morphology of the microneedles was examined with a field-emission SEM. (For further details, see the Supplementary Materials.)

SUPPLEMENTARY MATERIALS

Supplementary material for this article is available at http://advances.sciencemag.org/cgi/content/full/3/3/e1601314/DC1

Supplementary Text

fig. S1. Optical camera images of the wearable diabetes patch.
fig. S2. Device fabrication process.
fig. S3. Schematic illustration of the operation sequence of the diabetes treatment system.
fig. S4. Electrochemical analysis of the planar and porous gold electrode.
fig. S5. Drug delivery from microneedles with integrated heaters.
fig. S6. Effect of the sweat control layers and miniaturization of the glucose sensor.
fig. S7. Characterization of the glucose sensor.
fig. S8. Characterization of the pH sensor.
fig. S9. Skin temperature and characterization of chlorpropamide-loaded PCNs.
fig. S10. Characterization of hyaluronic acid, DOPA-conjugated hyaluronic acid.
fig. S11. Characterization of the PCNs.
fig. S12. Fabrication process of the microneedles.
fig. S13. Characterization of the heater and temperature sensor and their cooperation.
fig. S14. Portable electrochemical analyzer for the wearable diabetes patch.
fig. S15. Reliability of the wearable diabetes patch under variable skin temperature and multiple reuses.
fig. S16. Sweat uptake and calibration of the disposable strip-type sensors.
fig. S17. Human sweat analysis.
fig. S18. Feedback microneedle therapy.

REFERENCES AND NOTES

1. D. R. Whiting, L. Guariguata, C. Weil, J. Shaw, IDF diabetes atlas: Global estimates of the prevalence of diabetes for 2011 and 2030. *Diabetes Res. Clin. Pract.* **94**, 311–321 (2011).
2. The Diabetes Control and Complications Trial Research Group, The effect of intensive treatment of diabetes on the development and progression of long-term complications in insulin-dependent diabetes mellitus. *N. Engl. J. Med.* **329**, 977–986 (1993).
3. A. J. Bandodkar, W. Jia, C. Yardimci, X. Wang, J. Ramirez, J. Wang, Tattoo-based noninvasive glucose monitoring: A proof-of-concept study. *Anal. Chem.* **87**, 394–398 (2015).
4. W. Gao, S. Emaminejad, H. Y. Nyein, S. Challa, K. Chen, A. Peck, H. M. Fahad, H. Ota, H. Shiraki, D. Kiriya, D.-H. Lien, G. A. Brooks, R. W. Davis, A. Javey, Fully integrated wearable sensor arrays for multiplexed in situ perspiration analysis. *Nature* **529**, 509–514 (2016).
5. H. Lee, T. K. Choi, Y. B. Lee, H. R. Cho, R. Ghaffari, L. Wang, H. J. Choi, T. D. Chung, N. Lu, T. Hyeon, S. H. Choi, D.-H. Kim, A graphene-based electrochemical device with

thermoresponsive microneedles for diabetes monitoring and therapy. *Nat. Nanotechnol.* **11**, 566–572 (2016).
6. O. Veiseh, R. Langer, Diabetes: A smart insulin patch. *Nature* **524**, 39–40 (2015).
7. J. Yu, Y. Zhang, Y. Ye, R. DiSanto, W. Sun, D. Ranson, F. S. Ligler, J. B. Buse, Z. Gu, Microneedle-array patches loaded with hypoxia-sensitive vesicles provide fast glucose-responsive insulin delivery. *Proc. Natl. Acad. Sci. U.S.A.* **112**, 8260–8265 (2015).
8. S. Imani, A. J. Bandodkar, A. M. V. Mohan, R. Kumar, S. Yu, J. Wang, P. P. Mercier, A wearable chemical–electrophysiological hybrid biosensing system for real-time health and fitness monitoring. *Nat. Commun.* **7**, 11650 (2016).
9. J. Kim, I. Jeerapan, S. Imani, T. N. Cho, A. Bandodkar, S. Cinti, P. P. Mercier, J. Wang, Noninvasive alcohol monitoring using a wearable tattoo-based iontophoretic-biosensing system. *ACS Sens.* **1**, 1011–1019 (2016).
10. H. Y. Y. Nyein, W. Gao, Z. Shahpar, S. Emaminejad, S. Challa, K. Chen, H. M. Fahad, L.-C. Tai, H. Ota, R. W. Davis, A. Javey, A wearable electrochemical platform for noninvasive simultaneous monitoring of Ca^{2+} and pH. *ACS Nano* **10**, 7216–7224 (2016).
11. W. Gao, H. Y. Y. Nyein, Z. Shahpar, H. M. Fahad, K. Chen, S. Emaminejad, Y. Gao, L.-C. Tai, H. Ota, E. Wu, J. Bullock, Y. Zeng, D.-H. Lien, A. Javey, Wearable microsensor array for multiplexed heavy metal monitoring of body fluids. *ACS Sens.* **1**, 866–874 (2016).
12. J. Moyer, D. Wilson, I. Finkelshtein, B. Wong, R. Potts, Correlation between sweat glucose and blood glucose in subjects with diabetes. *Diabetes Technol. Ther.* **14**, 398–402 (2012).
13. K. Sakaguchi, Y. Hirota, N. Hashimoto, W. Ogawa, T. Hamaguchi, T. Matsuo, J.-I. Miyagawa, M. Namba, T. Sato, S. Okada, Evaluation of a minimally invasive system for measuring glucose area under the curve during oral glucose tolerance tests: Usefulness of sweat monitoring for precise measurement. *J. Diabetes Sci. Technol.* **7**, 678–688 (2013).
14. S. K. Vashist, Non-invasive glucose monitoring technology in diabetes management: A review. *Anal. Chim. Acta* **750**, 16–27 (2012).
15. M. J. Tierney, H. L. Kim, M. D. Burns, J. A. Tamada, R. O. Potts, Electroanalysis of glucose in transcutaneously extracted samples. *Electroanalysis* **12**, 666–671 (2000).
16. M. Kaltenbrunner, T. Sekitani, J. Reeder, T. Yokota, K. Kuribara, T. Tokuhara, M. Drack, R. Schwödiauer, I. Graz, S. Bauer-Gogonea, S. Bauer, T. Someya, An ultra-lightweight design for imperceptible plastic electronics. *Nature* **499**, 458–463 (2013).
17. T. Sekitani, U. Zschieschang, H. Klauk, T. Someya, Flexible organic transistors and circuits with extreme bending stability. *Nat. Mater.* **9**, 1015–1022 (2010).
18. J. Kim, D. Son, M. Lee, C. Song, J.-K. Song, J. H. Koo, D. J. Lee, H. J. Shim, J. H. Kim, M. Lee, T. Hyeon, D.-H. Kim, A wearable multiplexed silicon nonvolatile memory array using nanocrystal charge confinement. *Sci. Adv.* **2**, e1501101 (2016).
19. D.-H. Kim, N. Lu, R. Ma, Y.-S. Kim, R.-H. Kim, S. Wang, J. Wu, S. M. Won, H. Tao, A. Islam, K. J. Yu, T.-i. Kim, R. Chowdhury, M. Ying, L. Xu, M. Li, H.-J. Chung, H. Keum, M. McCormick, P. Liu, Y.-W. Zhang, F. G. Omenetto, Y. Huang, T. Coleman, J. A. Rogers, Epidermal electronics. *Science* **333**, 838–843 (2011).
20. K.-I. Jang, H. U. Chung, S. Xu, C. H. Lee, H. Luan, J. Jeong, H. Cheng, G.-T. Kim, S. Y. Han, J. W. Lee, J. Kim, M. Cho, F. Miao, Y. Yang, H. N. Jung, M. Flavin, H. Liu, G. W. Kong, K. J. Yu, S. I. Rhee, J. Chung, B. Kim, J. W. Kwak, M. H. Yun, J. Y. Kim, Y. M. Song, U. Paik, Y. Zhang, Y. Huang, J. A. Rogers, Soft network composite materials with deterministic and bio-inspired designs. *Nat. Commun.* **6**, 6566 (2015).
21. D. Son, J. Lee, S. Qiao, R. Ghaffari, J. Kim, J. E. Lee, C. Song, S. J. Kim, D. J. Lee, S. W. Jun, S. Yang, M. Park, J. Shin, K. Do, M. Lee, K. Kang, C. S. Hwang, N. Lu, T. Hyeon, D.-H. Kim, Multifunctional wearable devices for diagnosis and therapy of movement disorders. *Nat. Nanotechnol.* **9**, 397–404 (2014).
22. J. Kim, M. Lee, H. J. Shim, R. Ghaffari, H. R. Cho, D. Son, Y. H. Jung, M. Soh, C. Choi, S. Jung, K. Chu, D. Jeon, S.-T. Lee, J. H. Kim, S. H. Choi, T. Hyeon, D.-H. Kim, Stretchable silicon nanoribbon electronics for skin prosthesis. *Nat. Commun.* **5**, 5747 (2014).
23. M. R. Prausnitz, R. Langer, Transdermal drug delivery. *Nat. Biotechnol.* **26**, 1261–1268 (2008).
24. UK Prospective Diabetes Study (UKPDS) Group, Effect of intensive blood-glucose control with metformin on complications in overweight patients with type 2 diabetes (UKPDS 34). *Lancet* **352**, 854–865 (1998).
25. M. Zhang, C. Liao, C. H. Mak, P. You, C. L. Mak, F. Yan, Highly sensitive glucose sensors based on enzyme-modified whole-graphene solution-gated transistors. *Sci. Rep.* **5**, 8311 (2015).
26. Y. Zhang, Y. Hu, G. S. Wilson, D. Moatti-Sirat, V. Poitout, G. Reach, Elimination of the acetaminophen interference in an implantable glucose sensor. *Anal. Chem.* **66**, 1183–1188 (1994).
27. Z. Niu, L. Liu, L. Zhang, Q. Shao, W. Zhou, X. Chen, S. Xie, A universal strategy to prepare functional porous graphene hybrid architectures. *Adv. Mater.* **26**, 3681–3687 (2014).
28. W. Wang, S. You, X. Gong, D. Qi, B. K. Chandran, L. Bi, F. Cui, X. Chen, Bioinspired nanosucker array for enhancing bioelectricity generation in microbial fuel cells. *Adv. Mater.* **28**, 270–275 (2016).
29. L. Pan, G. Yu, D. Zhai, H. R. Lee, W. Zhao, N. Liu, H. Wang, B. C.-K. Tee, Y. Shi, Y. Cui, Z. Bao, Hierarchical nanostructured conducting polymer hydrogel with high electrochemical activity. *Proc. Natl. Acad. Sci. U.S.A.* **109**, 9287–9292 (2012).
30. J. C. Claussen, A. Kumar, D. B. Jaroch, M. H. Khawaja, A. B. Hibbard, D. M. Porterfield, T. S. Fisher, Nanostructuring platinum nanoparticles on multilayered graphene petal nanosheets for electrochemical biosensing. *Adv. Funct. Mater.* **22**, 3399–3405 (2012).
31. A. Singh, M. Corvelli, S. A. Unterman, K. A. Wepasnick, P. McDonnell, J. H. Elisseeff, Enhanced lubrication on tissue and biomaterial surfaces through peptide-mediated binding of hyaluronic acid. *Nat. Mater.* **13**, 988–995 (2014).
32. S. Y. Yang, E. D. O'Cearbhaill, G. C. Sisk, K. M. Park, W. K. Cho, M. Villiger, B. E. Bouma, B. Pomahac, J. M. Karp, A bio-inspired swellable microneedle adhesive for mechanical interlocking with tissue. *Nat. Commun.* **4**, 1702 (2013).
33. X. Huang, Y. Liu, K. Chen, W.-J. Shin, C.-J. Lu, G.-W. Kong, D. Patnaik, S.-H. Lee, J. F. Cortes, J. A. Rogers, Stretchable, wireless sensors and functional substrates for epidermal characterization of sweat. *Small* **10**, 3083–3090 (2014).
34. D. P. Rose, M. E. Ratterman, D. K. Griffin, L. Hou, N. Kelley-Loughnane, R. R. Naik, J. A. Hagen, I. Papautsky, J. C. Heikenfeld, Adhesive RFID sensor patch for monitoring of sweat electrolytes. *IEEE Trans. Biomed. Eng.* **62**, 1457–1465 (2015).
35. C. J. Harvey, R. F. LeBouf, A. B. Stefaniak, Formulation and stability of a novel artificial human sweat under conditions of storage and use. *Toxicol. In Vitro* **24**, 1790–1796 (2010).
36. D. S. Young, D. W. Thomas, R. B. Friedman, L. C. Pestaner, *Effects of drugs on clinical laboratory tests* (AACC Press, ed.4, 1995). pp. 374–391.
37. Z. Tang, X. Du, F. R. Louie, J. G. Kost, Effects of drugs on glucose measurements with handheld glucose meters and a portable glucose analyzer. *Am. J. Clin. Pathol.* **113**, 75–86 (2000).
38. J. A. Hirst, A. J. Farmer, R. Ali, N. W. Roberts, R. J. Stevens, Quantifying the effect of metformin treatment and dose on glycemic control. *Diabetes Care* **35**, 446–454 (2012).
39. G. D. Moon, S.-W. Choi, X. Cai, W. Li, E. C. Cho, U. Jeong, L. V. Wang, Y. Xia, A new theranostic system based on gold nanocages and phase-change materials with unique features for photoacoustic imaging and controlled release. *J. Am. Chem. Soc.* **133**, 4762–4765 (2011).
40. M. R. Prausnitz, Microneedles for transdermal drug delivery. *Adv. Drug Deliv. Rev.* **56**, 581–587 (2004).
41. K. Nakamura, S. F. Morrison, A thermosensory pathway that controls body temperature. *Nat. Neurosci.* **11**, 62–71 (2008).
42. N. C. Sambol, J. Chiang, M. O'Conner, C. Y. Liu, E. T. Lin, A. M. Goodman, L. Z. Benet, J. H. Karam, Pharmacokinetics and pharmacodynamics of metformin in healthy subjects and patients with noninsulin-dependent diabetes mellitus. *J. Clin. Pharmacol.* **36**, 1012–1021 (1996).

Acknowledgments: All animal procedures were approved by the Institutional Animal Care and Use Committee (IACUC) of the Biomedical Research Institute of Seoul National University Hospital. All experiments were performed according to IACUC guidelines. The human sweat study was performed in compliance with the protocol approved by the institutional review board at the Seoul National University (IRB No. 1605/003-002). **Funding:** This work was supported by IBS-R006-D1. **Author contributions:** H.L., C.S., T.H., and D.-H.K. designed the experiments. H.L., C.S., Y.S.H., M.S.K., H.R.C., T.K., K.S., S.H.C., T.H., and D.-H.K. performed the experiments and analysis. H.L., C.S., T.H., and D.-H.K. wrote the paper. **Competing interests:** The authors declare that they have no competing interests. **Data and materials availability:** All data needed to evaluate the conclusions in the paper are present in the paper and/or the Supplementary Materials. Additional data related to this paper may be requested from the authors.

Submitted 10 June 2016
Accepted 2 February 2017
Published 8 March 2017
10.1126/sciadv.1601314

Citation: H. Lee, C. Song, Y. S. Hong, M. S. Kim, H. R. Cho, T. Kang, K. Shin, S. H. Choi, T. Hyeon, D.-H. Kim, Wearable/disposable sweat-based glucose monitoring device with multistage transdermal drug delivery module. *Sci. Adv.* **3**, e1601314 (2017).

ScienceAdvances
AAAS

Wearable/disposable sweat-based glucose monitoring device with multistage transdermal drug delivery module

Hyunjae Lee, Changyeong Song, Yong Seok Hong, Min Sung Kim, Hye Rim Cho, Taegyu Kang, Kwangsoo Shin, Seung Hong Choi, Taeghwan Hyeon and Dae-Hyeong Kim (March 8, 2017)

Sci Adv 2017, 3:.
doi: 10.1126/sciadv.1601314